Catalysis Letters (2021) 151:1592–1603
https://doi.org/10.1007/s10562-020-03411-9

Total Oxidation of Methane Over Sulfur Poisoning Resistant Pt/ZrO_2 Catalyst: Effect of Pt^{2+}–Pt^{4+} and Pt^{2+}–Zr^{4+} Dipoles at Metal-Support Interface

Rosalía Torralba[1] · Grisel Corro[1] · Fer Rosales[1] · Fortino Bañuelos[1] · Umapada Pal[2] · Octavio Olivares-Xometl[3] · Emmanuel Guilleminot[4] · José Luis G. Fierro[5]

Received: 10 May 2020 / Accepted: 22 July 2020 / Published online: 12 October 2020

Abstract

We present a Pt/ZrO_2 catalyst that can operate in the harsh conditions of methane oxidation without being deactivated by SO_2. XPS analysis of $1\%Pt/ZrO_2$ catalyst revealed the presence of stable Pt^{2+}–Pt^{4+} and Pt^{2+}–Zr^{4+} bifunctional catalytic sites of dipolar nature at the Pt–ZrO_2 interface. These sites increase the probability of CH_4 polarization, increasing the strength of their collision with the catalyst surface, lowering the C–H bond energy and facilitating the abstraction of the first hydrogen in adsorbed CH_4. The resistance of the catalyst to deactivation by sulfur poisoning is explained considering the stronger interaction of SO_2 with Pt^{2+}–Zr^{4+} dipolar sites, presenting a higher dipolar electric potential than Pt^{2+}–Pt^{4+}, on which CH_4 adsorption and oxidation occur.

Graphic Abstract

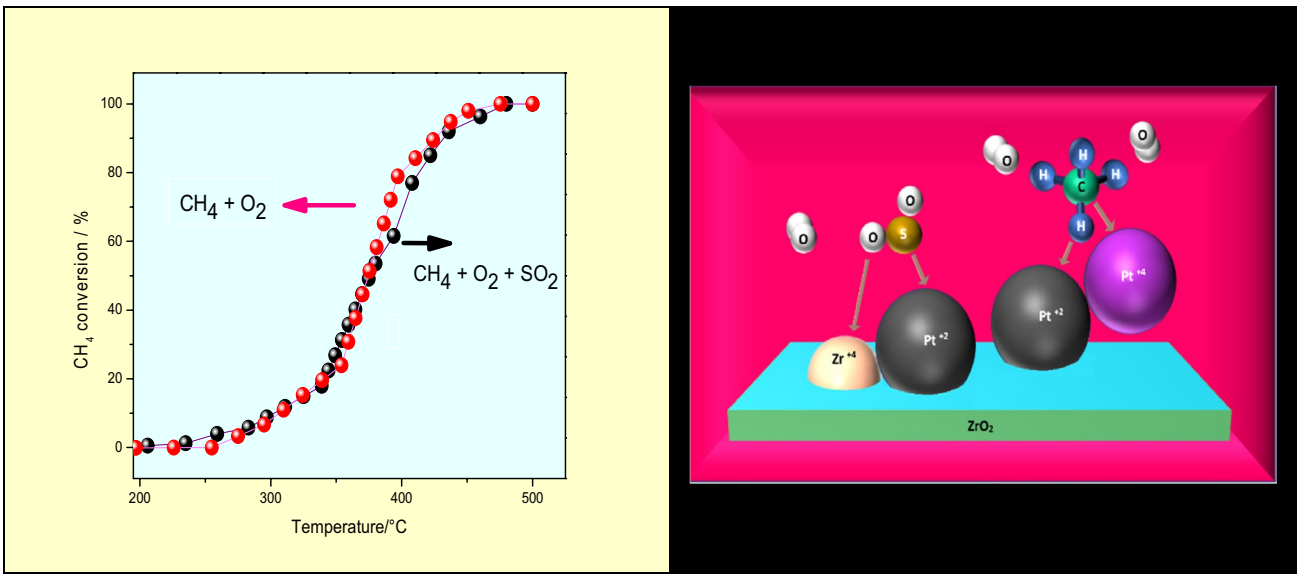

Keywords Pt/ZrO_2 · Methane oxidation · Natural gas engine · CH_4 emissions · SO_2

✉ Grisel Corro
griselda.corro@correo.buap.mx

Extended author information available on the last page of the article

1 Introduction

The automobile industries worldwide are increasingly inclined towards lean burn natural gas engines to utilize natural gas and biogas as the substitutes of conventional fossil fuels. The popularity of lean burn natural gas engines and dual fuel engines is strongly growing due to the low costs and high availability of natural gas and biogas. Shale gas is already available around the world [1, 2] and more vehicles are expected to operate using liquefied natural gas. These engines provide high fuel efficiency and emit relatively lower amounts of CO_2 than diesel or gasoline engines due to a higher H:C ratio in these gaseous fuels mostly consist of methane. Natural gas engines used in stationary and mobile applications have demonstrated lower SO_x, NO_x, and particulate matter emissions as compared to diesel engines. However, incomplete combustion results in high amounts of emissions of CH_4 which contributes strongly to the greenhouse effect. A great effort has been made to develop efficient catalysts for utilization in exhaust gas aftertreatment to lower the emission of CH_4 [3]. Significant methane conversion under typical exhaust-natural gas conditions is only achieved by noble metal-based catalysts, palladium showing the highest low temperature activity for total oxidation of methane [4–8]. The main challenge associated to the utilization of Pd-based catalysts is their poisoning by sulfur containing compounds present as odorizes in the natural gas or from lubricants used in the engine [8]. Thus, during natural gas combustion, SO_2 and H_2S, which are identified as strong poisons for Pd-based oxidation catalysts, are generated [9, 10]. At high temperature, under lean conditions, SO_2 leads to the formation of sulfites and sulfates on the noble metal and on the support [11, 12]. On the other hand, Pt is one of the most active metal catalysts for hydrocarbon oxidation, with activity comparable to Pd. Moreover, it is more sulfur tolerant than palladium [13, 14]. It has been reported that addition of Pt to Pd/Al_2O_3 improves the resistance of Pd to deactivation by sulfur poisoning [11, 15, 16]. However, the methane oxidation activity of Pd–Pt/Al_2O_3 decreased in presence of SO_2 in the reaction feed.

In this work, we present a Pt nanoparticle supported ZrO_2 catalyst and its methane oxidation behavior. The catalyst is highly resistant to sulfur deactivation, whose activity does not reduce even in presence of SO_2. Effects of ZrO_2 support on the active catalytic sites over small Pt particles for the total oxidation of methane in lean conditions have been studied. Effect of SO_2 in reaction gas on the catalytic activity of the catalyst has been evaluated analyzing the electronic states of Pt species before and after utilization in catalytic cycles, along with considering the mean size of Pt particles.

2 Experimental Section

2.1 Catalysts Preparation

We used commercial ZrO_2 powder (Sigma-Aldrich, 99.99%) to prepare Pt supported catalyst. The catalyst was prepared by impregnating the ZrO_2 powder with an aqueous solution of chloroplatinic acid hexahydrate ($H_2PtCl_6{\cdot}6H_2O$, Aldrich, 99.99%) of appropriate concentration to obtain nominal 1 wt% Pt/metal-oxide mixture. The suspension was magnetically stirred at room temperature for 1 h, recovered by filtration, and washed thoroughly to remove chlorine, and other unreacted species (if any). After drying at 120 °C overnight, the sample was calcined under air flow (100 ml min^{-1}) in a tubular furnace at 500 °C for 4 h. A linear heating ramp of 10 °C min^{-1} was utilized to reach the maximum temperature. After cooling down to room temperature, the catalyst, designated as 1%Pt/ZrO_2 was stored in dry conditions. A ZrO_2 sample without platinum ion impregnation was prepared in the same way to use as the reference.

2.2 Catalysts Characterization

N_2 adsorption–desorption isotherms of the catalysts were obtained using a Belsorp Mini II sorptometer. The specific surface area (S_g) of the samples was determined from their N_2 physisorptions at 77 K, using BET analysis. Before recording their adsorption–desorption isotherms, the samples (0.5 g each) were degassed at 400 °C for 2 h. After cooling to room temperature (25 °C), the isotherms were recorded in the pressure range 0.0–6.6 kPa. To determine the saturation uptake, the technique of back extrapolation of the linear portion of the isotherms to zero equilibrium pressure was applied.

The FTIR spectra of the catalysts before and after methane oxidation cycles in the presence and absence of SO_2 were recorded from 800 to 3500 cm^{-1} on a Bruker Vertex 70 spectrometer. For the FTIR measurement, 1 mg of the composite sample was mixed with 99 mg of dry KBr and compressed to make a circular pellet of about 5 mm diameter.

Diffuse reflectance spectra (DRS) of the catalysts before and after methane oxidation cycles were measured on dry-pressed disks (~15 mm diameter) using a Shimadzu UV–Vis spectrophotometer equipped with an integrating sphere, and $BaSO_4$ as standard reflectance material. The crystallinity and structural phase of the samples were verified through powder X-ray diffraction (XRD), using the CuK_α radiation ($\lambda = 1.5406$ Å) of a Bruker D8 Discover diffractometer.

X-ray photoelectron spectra (XPS) were recorded on 1%Pt/ZrO_2 catalysts before and after 6 methane oxidation cycles, using an Escalab 200R electron spectrometer equipped with a hemispherical analyzer, operating in a

constant pass energy mode. Monochromatic MgK_{α} emission ($h\nu = 1253.6$ eV) from the X-ray tube operating at 10 mA and 12 kV was utilized for recording the XPS spectra of the samples. Photoelectrons of specific energy regions of interest were scanned several times in order to obtain good signal-to-noise ratio. Intensities of the emission peaks were estimated by determining the area under each peak after subtracting an S-shaped background and fitting the experimental peak to Lorentzian/Gaussian curves (80%L/20%G). The peak positions of the elements were corrected utilizing the position of C*1s* peak coming from adventitious carbon appeared at 284.9 ± 0.2 eV.

High resolution transmission electron microscopic (HR-TEM) images of the $1\%Pt/ZrO_2$ catalyst before and after methane oxidation cycles were obtained in a JEOL JEM-ARM200CF microscope (lattice resolution 78 pm, acceleration voltage 200 kV). The samples for microscopic observation were prepared by dispersing the powder catalysts in ethanol and drop casting over carbon coated copper grids. The size distribution histogram of the platinum nanoparticles was prepared by measuring the size of 150–200 particles for each sample.

2.3 Catalytic Tests

All the catalytic tests were performed at 1 atm, in a continuous flow tubular quartz reactor of 10 mm inner diameter, placed inside a programmable furnace with internally mounted thermocouple. Reactant gases were fed from independent mass flow controllers. Methane oxidation tests over the catalysts were performed under a 100 ml min^{-1} flow rate of feed gas. Table 1 summarizes the composition of the feed gas used for the different processes.

The catalyst loaded in the reactor was of 200 mg diluted with 1.0 g of low surface area quartz (< 1 m^2 g^{-1}) to prevent heat transfer limitations. The reactor outflow was analyzed in a Shimadzu gas chromatograph, provided with a thermo-conductivity detector (TCD), to determine CH_4, CO, CO_2, and H_2O concentrations as a function of the reaction temperature. To determine the SO_2 evolution with reaction temperature, the reactor outflow was analyzed in a Bruker (Vertex 70) FTIR gas spectrometer provided with an analysis gas cell. The analysis was performed using the Galactic GRAMS-quantitative software which enabled the detection of SO_2. However, this system did not permit the quantitative determination of SO_3. Before performing the tests, the samples were pretreated in the reactant stream at 500 °C for 1 h. After which, they were cooled down (keeping in the reactant stream) to 25 °C.

Catalytic CH_4 oxidation process was studied by monitoring the evolution of methane conversion as a function of temperature (light-off curves). Catalytic oxidation of CH_4 was performed in the 25–500 °C temperature range, heating the catalysts at 2 °C min^{-1}. After test, the samples were cooled down to 25 °C. The whole process of methane oxidation from 25 to 500 °C was defined as a cycle. The catalysts were heated at 2 °C min^{-1} rate to allow enough time to reach a steady state at each of the measurement temperatures. To verify the stability of the catalysts, six similar cycles were performed over the same catalyst sample. Temperature-programmed reaction profiles allowed us to determine the temperature at which methane conversion attains 10% (T_{10}), 50% (T_{50}), and 100% (T_{100}).

3 Results and Discussion

3.1 Catalysts Characterization

3.1.1 Surface Area Analysis

Specific surface area of the fresh and used catalysts estimated from their N_2 adsorption–desorption isotherms is presented in Table 2. As can be seen, the specific surface area of the catalyst did not change significantly after its use in oxidation cycles.

3.1.2 FTIR Characterization of the Catalysts

Figure 1 presents FTIR spectra of the freshly prepared $1\%Pt/ZrO_2$, the $1\%Pt/ZrO_2$ catalyst after methane oxidation cycles, and the catalyst after methane oxidation cycles in presence of SO_2. All the spectra revealed an intense band in the 850–650 cm^{-1} range, with a well-defined peak around 748 cm^{-1}, corresponding to monoclinic zirconia [17, 18].

Table 1 Composition of the feed gases used for catalytic tests over the $1\%Pt/ZrO_2$ catalyst

Reaction	Feed gas composition (Volume %)			
	CH_4	O_2	SO_2	N_2
$CH_4 + O_2$	0.2	10	–	Balance
$CH_4 + O_2 + SO_2$	0.2	10	0.02	Balance

Table 2 Specific surface areas of the catalysts estimated from their N_2 adsorption–desorption isotherms recorded at 77 K

Catalyst	Specific surface area (m^2g^{-1})		
	Fresh sample	After oxidation cycles $CH_4 + O_2$	After oxidation cycles $CH_4 + O_2 + SO_2$
ZrO_2	67	67	60
$1\%Pt/ZrO_2$	57	54	52

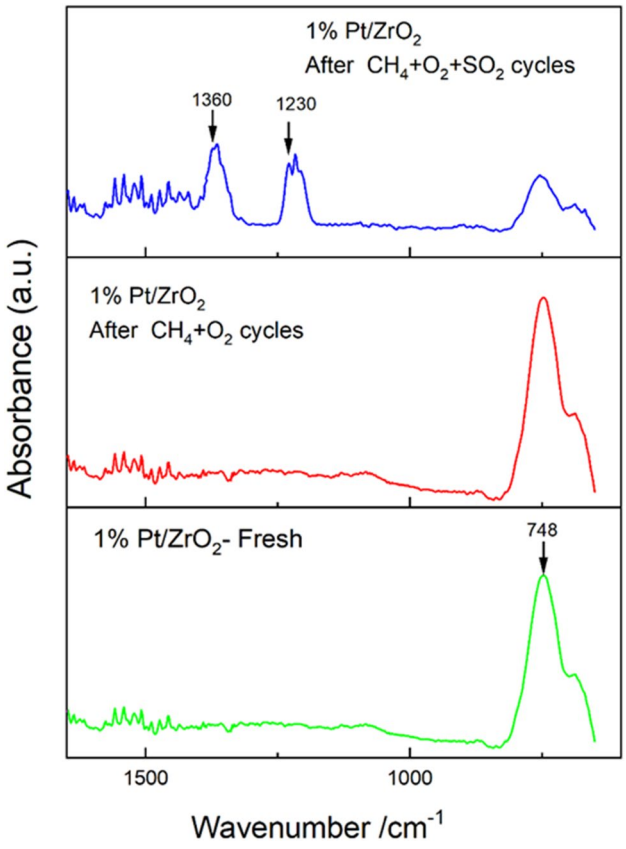

Fig. 1 FTIR spectra of the fresh 1%Pt/ZrO_2 catalyst, and the catalyst used in methane oxidation cycle in absence and presence of SO_2

In the spectrum of the catalyst utilized in methane oxidation cycles in presence of SO_2, there appeared two well defined bands in-between 1400 and 1200 cm^{-1}. The band peaked around 1360 cm^{-1} corresponds to the S=O stretching mode, which indicates the formation of zirconium sulfates in the sample [17–19]. Appearance of the second band peaked around 1230 cm^{-1} has been frequently associated to the surface sulfate species in sulfated zirconia [17, 18].

3.1.3 UV–Vis Characterization of the Catalysts

Figure 2 presents the UV–Vis DRS spectra of the ZrO_2 support and the 1%Pt/ZrO_2 catalyst fresh and after reactions. According to the spectra of the monoclinic ZrO_2, the absorption band appeared around 233 nm is associated to charge transfer from the anions to the cations (O^{2-}–Zr^{4+}) in ZrO_2 [20, 21]. The absorption spectrum of the fresh 1%Pt/ZrO_2 revealed an intense absorption signal at higher energy spreading from 200 and 300 nm which has been assigned to the overlapping of the absorption bands associated to the charge transfer from anions to the cations (O^{2-}–Zr^{4+}) in ZrO_2 and the charge transfer from chloride ligands to platinum in oxychloride surface complexes [PtO_xCl_y] [22–24].

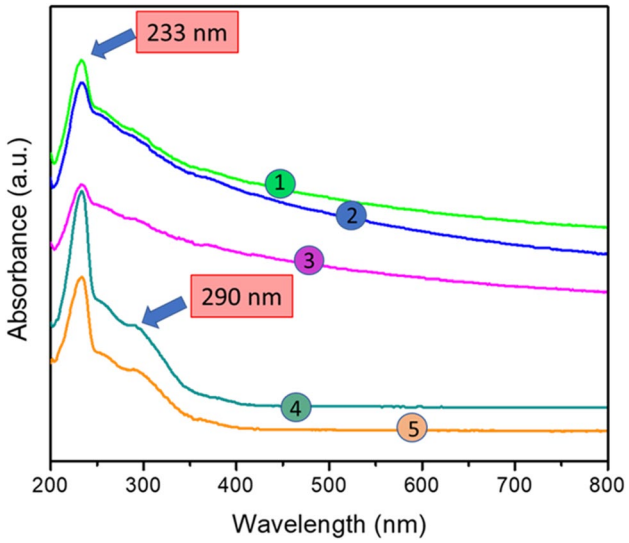

Fig. 2 Absorption spectra of (1) fresh 1%Pt/ZrO_2, (2) 1%Pt/ZrO_2 after methane oxidation cycles, (3) 1%Pt/ZrO_2 after methane oxidation cycles in presence of SO_2, (4) fresh ZrO_2, and (5) ZrO_2 after methane oxidation cycles in presence of SO_2

The broad band spreading between 270 and 400 nm could be attributed to d-d transitions in bulk compounds such as $PtO_x{\cdot}H_2O$ [22–24].

As can be seen in this figure, the absorption spectrum of 1%Pt/ZrO_2 catalyst, after use in oxidation cycles, revealed the same absorption signals as of the fresh (before use in methane oxidation cycles) catalyst, in the presence and in absence of SO_2. The results suggest that the same electronic states of the catalyst components prevail in 1%Pt/ZrO_2 even after six methane oxidation cycles, which may explain the high stability of the catalyst during methane oxidation cycles.

3.1.4 XPS Characterization of the Catalysts

XPS analysis was carried out on the fresh 1%Pt/ZrO_2 catalyst, after its use in methane oxidation cycles in absence and in presence of SO_2. Estimated binding energy (BE) values of Pt $4f_{7/2}$, Zr $3d_{5/2}$, S $2p$, and atomic percentages of Pt species in different oxidation states are presented in Table 3.

The core level Pt $4f_{7/2}$ emission revealed two components located around 73.1 and 75.3 eV, corresponding to Pt^{2+} and Pt^{4+} states, respectively (Fig. 3) [25–28]. The XPS estimated Pt/Zr ratio in the fresh catalyst (Table 3) indicates about 14% of the Zr surface atoms is covered by platinum species. It is interesting to note that after six methane oxidation cycles in the presence or absence of SO_2 in the reaction feed, the position of Pt $4f_{7/2}$ emission band remained almost same. This result indicates a very high electronic stability of surface Pt species during oxidation reactions. The Pt/Zr

Table 3 Binding energy positions of the components and Pt/Zr and S/Zr atomic ratios at the surface of the catalysts before (fresh), after using them in 6 methane oxidation cycles (used), and after using them in 6 methane oxidation cycles in the presence of SO_2

Catalyst	Pt $4f_{7/2}$ (eV)	Zr $3d_{5/2}$ (eV)	S 2p (eV)	Atomic ratio	
				Pt/Zr	S/Zr
1%Pt/ZrO_2 (fresh)	73.1 (69) 75.2 (31)	182.2		0.141	–
1%Pt/ZrO_2 (used)	73.1 (69) 75.2 (31)	182.1		0.145	–
1%Pt/ZrO_2 (used, in presence SO_2)	72.9 (61) 75.0 (39)	182.5	168.8	0.140	0.041

The % peak area of Pt^{2+}, and Pt^{4+} components are presented in parentheses

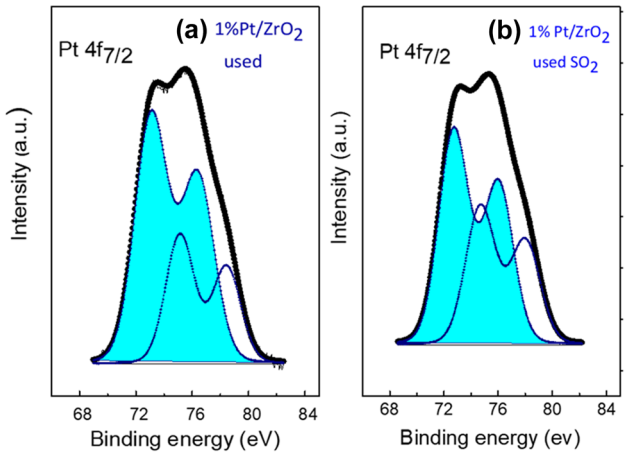

Fig. 3 Pt $4f_{7/2}$ core level XPS spectra of the 1%Pt/ZrO_2 catalyst after its use in 6 methane oxidation cycles **a** in absence, and **b** in presence of SO_2

atomic ratio remained almost same after the methane oxidation cycles in presence or absence of SO_2. Pt^{2+}/Zr and Pt^{4+}/Zr atomic ratios at the surface of the fresh and all used catalysts estimated, considering the % peak areas of Pt^{2+} and Pt^{4+} components, and the measured Pt/Zr atomic ratios are presented in Table 4. In this table, it can be observed, the estimated Pt^{2+}/Pt^{4+} ratio at the catalyst surface before and after oxidation cycles. These values show that after methane oxidation cycles performed in presence or absence of SO_2, the Pt^{2+}/Pt^{4+} ratio at the surface of the catalyst remained almost same, and hence the number of Pt^{2+}–Pt^{4+} catalytic sites at the surface of the catalyst.

The XPS spectrum of 1%Pt/ZrO_2 after 6 oxidation cycles revealed a single component Zr $3d_{5/2}$ emission band located around 182.2 eV, which corresponds to Zr^{4+} state [25, 29, 30]. However, after methane oxidation cycles in presence of SO_2, the signal revealed at slightly higher binding energy (182.5 eV), probably due to the formation of zirconium sulfate. This assumption is supported by the FTIR results presented in Fig. 1, showing the formation of zirconium sulfate during methane oxidation cycles in presence of SO_2.

3.1.5 HR-TEM Analysis of the Catalyst

Figure 4 shows typical high and low-resolution TEM images of the 1%Pt/ZrO_2 catalyst after 6 methane oxidation cycles in absence of SO_2. The size of the formed platinum particles varied between 1 and 2.5 nm, with average ~ 1.61 ± 0.45 nm (Fig. 5). It is interesting to note that the average size of Pt particle in the catalyst increased only marginally (~ 1.8 ± 0.59 nm) after 6 methane oxidation cycles performed in presence of SO_2.

The results indicate the Pt nanoparticles formed over ZrO_2 remain stable, probably due to ZrO_2 stabilization effect against sintering in oxidizing environment, as has been observed by Deeba et al. for platinum on silica, promoted by zirconium oxide [31].

3.2 Methane Oxidation Over the Catalysts

The evolution of CH_4 conversion with reaction temperature, during the 1st, 3rd and 6th oxidation cycles, performed in absence of SO_2, over 1%Pt/ZrO_2 are presented in Fig. 5. CH_4 conversion in the 25–500 °C temperature range over pristine ZrO_2 (results not shown) revealed very low methane conversion during the first and subsequent oxidation cycles. However, the conversion of CH_4 was high for the 1%Pt/ZrO_2

Table 4 Pt/Zr, Pt^{2+}/Zr, Pt^{4+}/Zr, and Pt^{2+}/Pt^{4+} atomic ratios at the surface of the fresh and all the used catalysts estimated considering the % peak areas of Pt^{2+} and Pt^{4+} components, and the measured Pt/Zr atomic ratios

Catalyst	Pt $4f_{7/2}$ (eV)	Pt^x	Atomic ratio			
			Pt/Zr	Pt^{2+}/Zr	Pt^{4+}/Zr	Pt^{2+}/Pt^{4+}
1%Pt/ZrO_2 (fresh)	73.1 (69) 75.2 (31)	Pt^{2+} Pt^{4+}	0.148	0.100	0.047	2.12
1%Pt/ZrO_2 (used)	73.1 (69) 75.2 (31)	Pt^{2+} Pt^{4+}	0.145	0.094	0.050	1.88
1%Pt/ZrO_2 (used SO_2)	72.7 (61) 74.7 (39)	Pt^{2+} Pt^{4+}	0.140	0.088	0.051	1.72

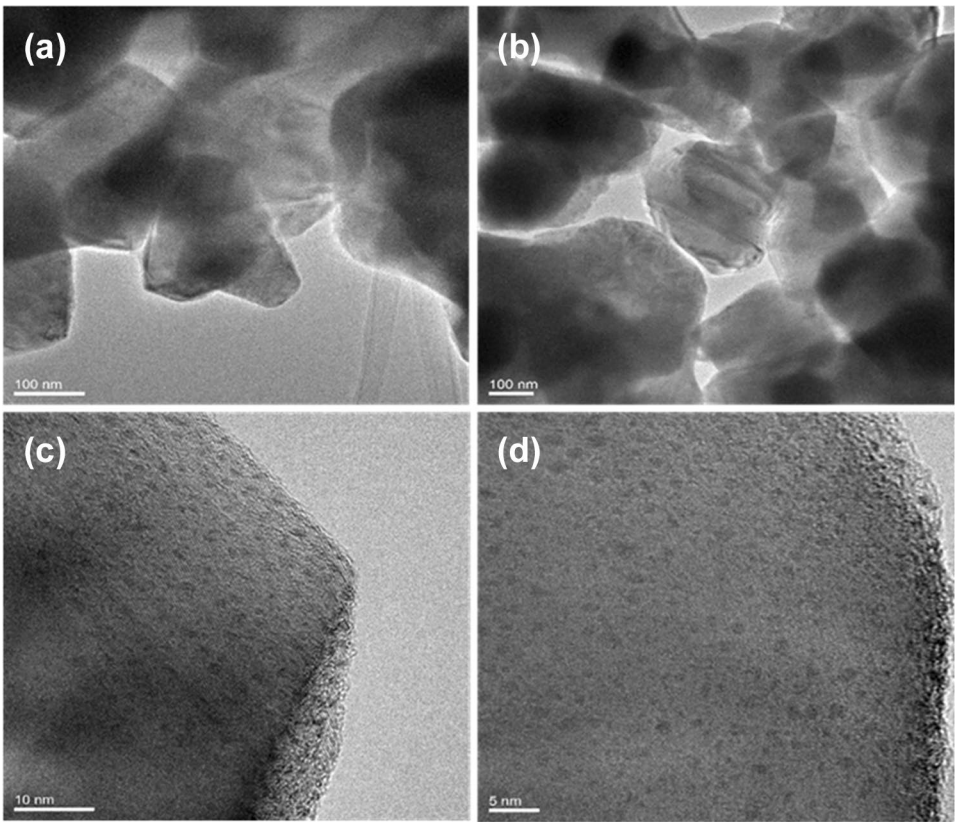

Fig. 4 Typical TEM images of 1%Pt/ZrO_2 catalyst **a** after 6 methane oxidation cycles, **b** after 6 methane oxidation cycles in presence of SO_2. HRTEM images **c** after 6 methane oxidation cycles, **d** after 6 methane oxidation cycles in presence of SO_2

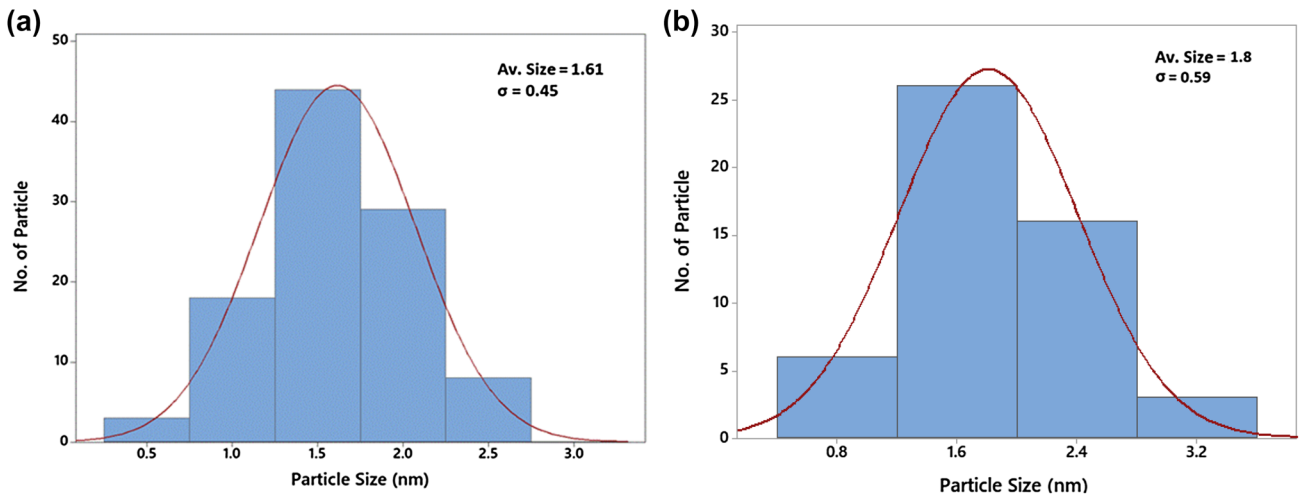

Fig. 5 Size distribution histograms and corresponding Gaussian fits for the Pt particles formed at the surface of ZrO_2 **a** after 6 methane oxidation cycles, **b** after 6 methane oxidation cycles in presence of SO_2

catalyst. The values calculated from the light-off curves, led to the construction of Table 5 which summarizes the T_{10}, T_{50}, and T_{100} values obtained for the conversion of CH_4 in CH_4–O_2 reaction. As can be seen in the table, the temperatures of 10% (T_{10}), 50% (T_{50}), and 100% (T_{100}) methane conversion over the catalyst remained almost same during the six oxidation cycles.

To study long-term stability of 1%Pt/ZrO_2, after the 6 methane oxidation cycles, the catalyst was heated at 500 °C in the reaction flow (0.2% CH_4, 10% O_2) for 30 h, after which an additional CH_4–O_2 reaction cycle was performed over the sample. The T_{50} values estimated for the different CH_4 oxidation cycles (Fig. 6) are presented in Table 5. As can be seen, the T_{50} values for methane oxidation remained

Table 5 Temperatures of 10% conversion (T_{10}), 50% conversion (T_{50}), and 100% conversion (T_{100}) for methane oxidation over 1%Pt/ZrO_2 catalyst

Reaction feed	Cycle	Temperature °C		
		T_{10}	T_{50}	T_{100}
CH_4+O_2				
	1st	312	369	497
	3rd	306	372	500
	6th	305	374	486
	After 30 h reaction 500 °C	312	380	500
$CH_4+O_2+SO_2$				
	1st	299	374	485
	3rd	299	380	488
	6th	311	393	500
	After 30 h reaction 500 °C	310	395	505

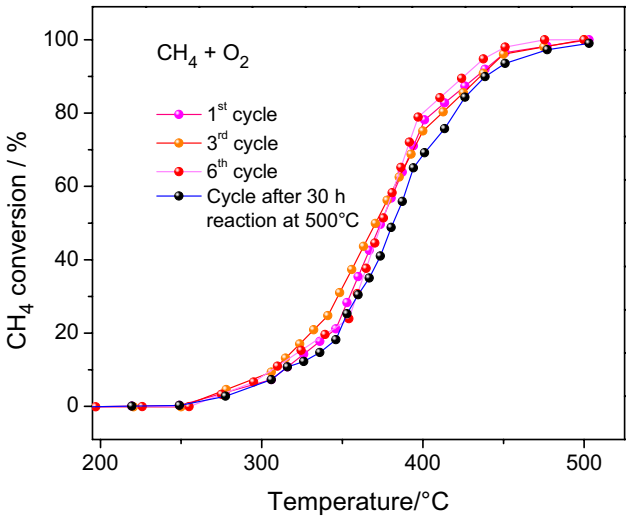

Fig. 6 Methane conversion over 1%Pt/ZrO_2 catalyst as a function of reaction temperature, in absence of SO_2

rather unaffected even after the long-term exposure of the catalyst to the reaction feed, indicating high stability of the 1%Pt/ZrO_2 catalyst for methane oxidation reaction.

The evolution of CH_4 conversion with reaction temperature over the 1%Pt/ZrO_2 catalyst during the 1st, 3rd and 6th methane oxidation cycles, performed in presence of SO_2 are presented in Fig. 7. For the long-term SO_2 exposure study, the catalyst used in 6 methane oxidation cycles in presence of SO_2 was heated at 500 °C in the reaction flow (0.2% CH_4, 10% O_2, and 0.02% SO_2) for further 30 h; after which an additional CH_4-O_2 reaction cycle was performed in the presence of 0.02% SO_2. The T_{50} values estimated for the different CH_4 oxidation cycles (Fig. 7) are presented in Table 5. As can be noticed, the T_{50} values for methane conversion

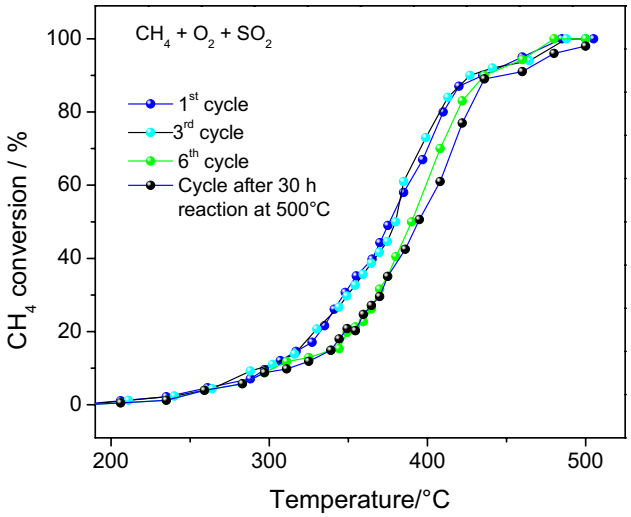

Fig. 7 Methane conversion over 1%Pt/ZrO_2 catalyst in presence of SO_2 as a function of reaction temperature

increased marginally during the first 6 methane oxidation cycles, indicating a slight deactivation of the catalyst. Nevertheless, the T_{50} measured after the long-term exposure of the catalyst to the reaction feed, remained same as estimated for the 6th oxidation cycle, indicating that the catalyst had attained a steady state activity after 6 oxidation cycles, and a long-lasting sulfur tolerance had been established.

3.3 SO_2 Reactions Over 1%Pt/ZrO_2 Catalyst During Methane Oxidation

During $CH_4+SO_2+O_2$ reactions over 1%Pt/ZrO_2, SO_2 may interact with the other reactants and with the catalyst. It is well known that the oxidation of SO_2 is catalyzed by Pt at temperatures higher than 200 °C, following the reaction [32–34]:

$$SO_2 + 1/2O_2 \rightarrow SO_3 \quad (1)$$

The generated SO_3 may react with the ZrO_2 support to form $ZrSO_4$. This assumption is supported by the results obtained from the XPS analysis of the 1%Pt/ZrO_2 after methane oxidation cycles in presence of SO_2, which revealed the formation of sulfates at its surface. FTIR spectrum of the sample also revealed absorption bands corresponding to zirconium sulfate. Now, ZrO_2 can possibly take up considerable amounts of SO_3 but this would be until all surface ZrO_2 sites had reacted with SO_3, generating surface zirconium sulfate.

In order to determine the reasons of the stability of 1%Pt/ZrO_2 methane oxidation activity in presence of SO_2, we have investigated the evolution of SO_2 conversion as a function of temperature during the methane oxidation cycles. Results are presented in Fig. 8. In the figure, it can be noticed that

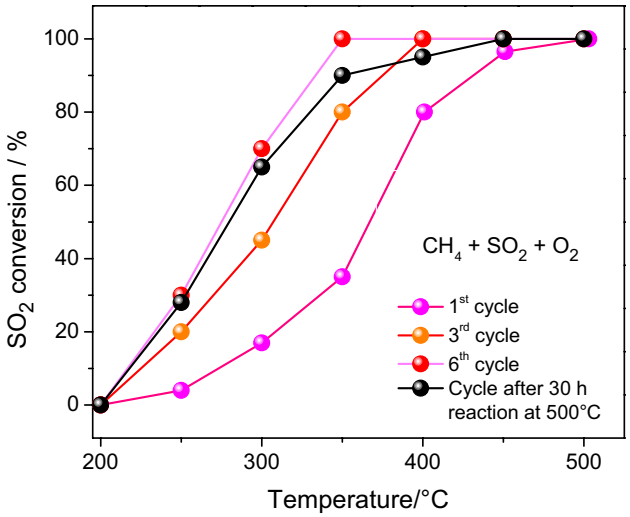

Fig. 8 SO_2 conversion over 1%Pt/ZrO_2 catalyst at different temperatures. During CH_4 oxidation over 1%Pt/ZrO_2 in presence of SO_2

the activity of the catalyst for SO_2 oxidation increases during the first few oxidation cycles. The highest conversion as a function of temperature, was achieved in the 6th oxidation cycle. After the long-term exposure of the catalyst to $CH_4 + SO_2 + O_2$ reaction feed, the evolution of SO_2 conversion with temperature remained nearly same as obtained in the 6th cycle (before the long-term exposure of the catalyst). The results suggest that the activity of the catalyst for SO_2 oxidation is promoted by the generation of new catalytic sites developed over Pt/ZrO_2 catalyst during the first few cycles. The new sites probably are mainly the sulfates formed over ZrO_2 surface.

It is well known that sulfated Pt/ZrO_2 (Pt/ZrO_2–$SO_4^=$) presents stronger surface acidity than a non-sulfated Pt/ZrO_2 catalyst [35]. The difference in surface acidity influences the adsorption–desorption properties of the catalysts, affecting their performance. SO_2 and SO_3 molecules are acidic. The adsorption of these molecules is therefore likely to become weaker on Pt/ZrO_2–$SO_4^=$ than on Pt/ZrO_2. Weakening steadily SO_2 molecule adsorption strength on Pt/ZrO_2–$SO_4^=$ would result in a steadily increase of the catalytic activity for the reaction (1) due to higher mobility of SO_2 molecules on the catalyst surface. The SO_2 oxidation process would have continued until the whole surface of the catalyst would be covered by zirconium sulfates. Thereafter, the SO_3 formed by oxidation of SO_2 catalyzed by Pt, not finding a free catalytic site to form sulfates, would have been carried away through the gas outflow.

It is well known that SO_3 is a toxic pollutant with strong effects on human health [36]. To prevent the emission of this hazardous gas to atmosphere, an additional reaction system preferably containing ZrO_2 or other active metal oxide catalyst such as Al_2O_3, BaO or CeO_2 can be placed in the downstream which can adsorb and react with the SO_3 present in the gas outflow, forming $ZrSO_4$. This additional reaction system (containing ZrO_2, Al_2O_3, BaO or CeO_2) would also be required to ensure that other excellent methane oxidation catalytic systems such as Pt/Al_2O_3, do not emit SO_3 to the atmosphere. This system should be replaced periodically, and the generated $ZrSO_4$ should be recovered for being utilized as a catalyst for acid/base reactions [37].

Although we could not quantify the SO_3 using Galactic GRAMS quantitative software in our FTIR gas spectrometer, the absorption spectra obtained during the 3rd–6th cycles, and the reaction cycle after the long-term exposure of the catalyst to methane-oxygen-SO_2 reaction feed revealed (results not shown) a signal around 1400 cm^{-1}, that increased from cycle to cycle. The signal (at 1400 cm^{-1}) has been frequently assigned to SO_3 in the literature [38, 39].

The obtained results suggest that zirconium sulfate formed over the catalyst surface does not deactivate the active sites for methane oxidation, and hence SO_2 in the reaction feed has no poisoning effect on the methane oxidation reaction in the studied temperature range (Fig. 7). As can be noted in Table 5, the T_{10}, T_{50}, and T_{100} values obtained for methane conversion after long term exposures of the catalyst to the reaction flow in presence of SO_2 are slightly higher than the corresponding values obtained in absence of SO_2 indicating a slight deactivation of the catalyst, which might have occurred due to its sulfation in presence of SO_2. However, the average size of the Pt particles (Fig. 5) also increased from 1.6 to 1.8 nm after 6 methane oxidation cycles performed in presence of SO_2. So, the marginally lower methane oxidation activity of the catalyst after prolonged high temperature exposure in SO_2 ambient, might also be due to temperature-induced growth of Pt nanoparticles.

3.4 Mechanistic Considerations of CH_4 Oxidation Over 1%Pt/ZrO_2

In general, methane oxidation is seen to follow the Mars-van Krevelen reduction–oxidation pathways [40], where the rate determining step is the abstraction of the first hydrogen on adsorbed methane molecule [41, 42]. Burch et al. considered the possibility of a more efficient activation of the C–H bond, through the polarization of methane molecule on a platinum surface covered partially by oxygen molecules [43]. On the other hand, Beck et al. observed that oxidation of methane over 1%Pt/γ–Al_2O_3 catalyst depends strongly on the size of Pt nanoparticles [44]. While the maximum turnover frequency was observed for Pt particles of ~ 2 nm average size, the catalyst contained a comparable amount of platinum species in different oxidation states. Although the high activity of those Pt-supported catalysts has been associated to the size of Pt particles, their specific crystallographic

planes, and other parameters, the results indicate an activation of the C–H bond over platinum surface containing Pt^{x}–Pt^{y} sites that can polarize CH_4 molecules, decreasing the C–H bond energy.

In this investigation, XPS study of the 1%Pt/ZrO_2 catalyst used for $CH_4 + O_2$ reaction cycles, revealed the presence of Pt^{2+}–Pt^{4+} dipolar catalytic sites at its surface. The number and nature of these dipolar sites remain unaffected despite the strong oxidation conditions and high temperature of the reaction. Repeated reaction cycles, and presence of SO_2 in the reaction feed did not have significant adverse effect on the performance of the catalyst.

While the formation of Pt^0 was reported previously in Pt/ZrO_2 catalyst prepared by similar process (utilized in the present work) after its utilization in CH_4 oxidation [44], XPS analysis revealed the presence of 69% PtO, and 31% PtO_2 (Tables 3, 4) in our 1%Pt/ZrO_2 catalyst after utilization in 6 cycles of CH_4 oxidation. It must be noted that while the Pt particles in the Pt/ZrO_2 catalyst of Ono et al. [45] were of ~ 3 nm size, the average size of the Pt particles in our 1%Pt/ZrO_2 catalyst was ~ 1.61 ± 0.45 nm, even after utilizing the catalyst in 6 oxidation cycles. It is well known that small metal nanoparticles can present electron deficiencies due to metal-support interactions [46, 47]. Indeed, Pt^0 was not detected in our catalyst, probably due to very small size of the platinum nanoparticles formed at Pt–ZrO_2 interface, probably due to electron transfer from Pt (Pt^0) to ZrO_2 support, generating surface Pt^{2+}, and resulting in the formation of Pt^{2+}–Pt^{4+} dipolar moieties. The same electron transfer process also generates stable Pt^{2+}–Zr^{4+} dipolar sites at the platinum–zirconia interface (Fig. 9).

Based on these facts, we propose two catalytic site models at the catalyst surface. The first site model involves Pt^{2+} sites at the Pt–ZrO_2 interface and surface Pt^{4+} sites in close proximity to Pt^{2+}. The second model is built with Pt^{2+} and Zr^{4+} moieties at the Pt–ZrO_2 interface.

The developed bifunctional catalytic sites (Pt^{2+}–Pt^{4+} and Pt^{2+}–Zr^{4+}) can strongly polarize CH_4 molecule, lowering the C–H bond energy, and facilitating the abstraction of the first hydrogen on the adsorbed methane by a heterolytic splitting of C–H bond.

Now, the potential of an electric dipole (φ) can be calculated using the relation:

$$\varphi = \frac{q_1 - q_2}{4\pi\varepsilon_0 r}$$

where q_1 and q_2 are the charges corresponding to the 1st and 2nd ion, respectively, separated by a distance r, and ε_0 is the vacuum permittivity. In Table 6, we enlist, (considering r as the sum of the radii of the possible charged species at the catalyst surface) the estimated values of potentials of the electric dipoles.

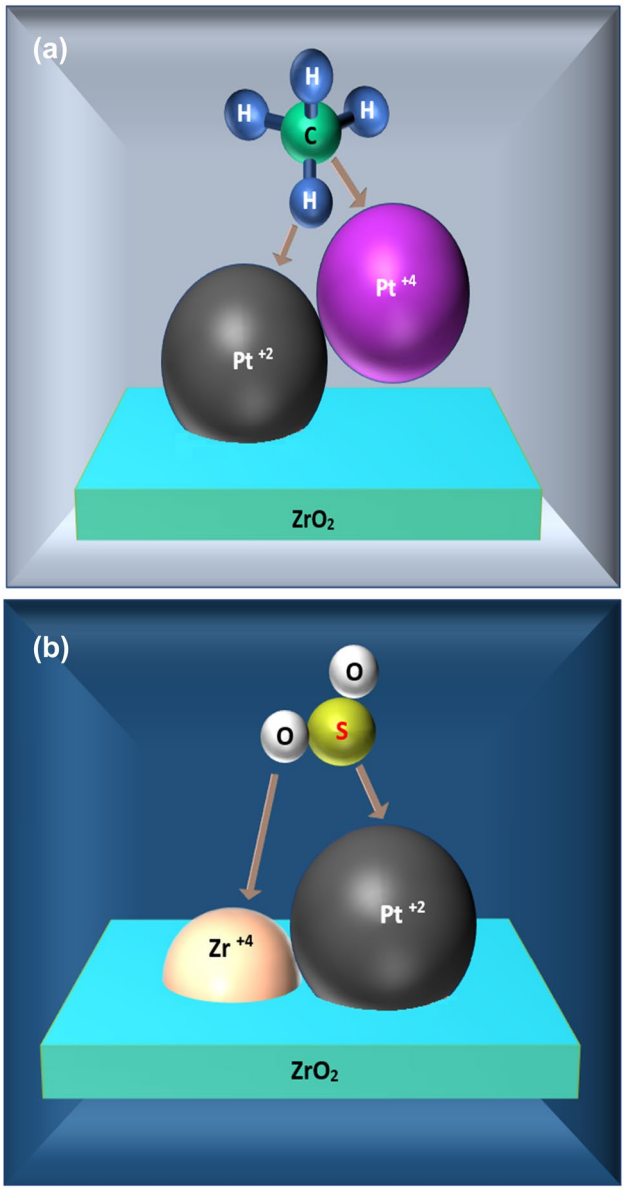

Fig. 9 Proposed catalytic site models at the platinum-zirconia interface

As can be seen in Table 6, Pt^{2+}–Zr^{4+} presents higher electric dipole potential than Pt^{2+}–Pt^{4+}. Therefore, the probability of CH_4 polarization would be higher on Pt^{2+}–Zr^{4+} than on Pt^{2+}–Pt^{4+}.

Now, in the CH_4–O_2 reaction conditions (excess oxygen, 25–500 °C), platinum surface should be fully covered by oxygen molecules of the reaction atmosphere, preventing CH_4 adsorption. However, CH_4 is polarized and adsorbed on Pt^{2+}–Pt^{4+} and Pt^{2+}–Zr^{4+} dipolar sites. In fact, the rate of CH_4 adsorption at the dipolar sites would be much higher than that of O_2 due to the methane non-zero polarizability [48]. On the other hand, as the O_2 molecules are not polarizable (zero polarizability), their

Table 6 Electric dipole potentials estimated for different possible bifunctional sites

Catalytic site	Ionic radio (r_i) (pm)				r (r_1+r_2) (pm)	q_1-q_2 (C)	$\varphi(4\pi\varepsilon_0)=(q_1-q_2)/r$ (C/pm)
	Pt^0	Pt^{2+}	Pt^{4+}	Zr^{4+}			
Pt^0–Pt^{2+}	177	94			271	2	0.0078
Pt^{2+}–Pt^{4+}		94	76.5		170.5	2	0.0117
Pt^{2+}–Zr^{4+}		94		73	167.0	2	0.0119
Pt^{4+}–Zr^{4+}			76.5	73	149.5	0	0.0

kinetic energy will not be affected by the field generated by the dipolar sites. Consequently, the CH_4 molecules, presenting an electric dipole moment of 5.38×10^{-6} D, will be rapidly attracted to these sites and adsorbed before and more strongly than O_2 molecules.

As can be seen in Figs. 6, 7 and Table 5, the $1\%Pt/ZrO_2$ catalyst is not deactivated by sulfur poisoning during methane oxidation in the presence of SO_2 in the reaction feed. Even after 6 methane oxidation cycles, the methane oxidation activity remained almost same. Also, the XPS results revealed that during methane oxidation cycles in presence of SO_2, the platinum Pt^{2+}–Pt^{4+} dipolar sites remained unaffected. This result indicates that the adsorption rate of CH_4 molecules on these sites should be almost unaffected despite the presence of SO_2. Nevertheless, SO_2, presenting an electric dipole moment of 1.633 D [49], higher than that of CH_4, (5.38×10^{-6} D), should have been strongly polarized by the Pt^{2+}–Pt^{4+} dipolar sites, and a higher adsorption rate compared to that of CH_4 should have taken place. Consequently, the methane oxidation rate should have decreased. However, this was not the case. This apparently contradictory result can be explained considering the presence of Pt^{2+}–Zr^{4+} dipolar sites at the catalyst surface, which present a higher electric dipole potential than Pt^{2+}–Pt^{4+}. Therefore, the probability of SO_2 polarization and consequent adsorption rate may be higher on Pt^{2+}–Zr^{4+} than on Pt^{2+}–Pt^{4+}. Adsorbed SO_2 on Pt^{2+}–Zr^{4+} dipolar sites may follow further oxidation reactions permitted by the thermodynamic parameters of the process, independently of CH_4 reactions at the catalyst surface. Accordingly, the probability of CH_4 adsorption on free Pt^{2+}–Pt^{4+} dipolar sites would remain unaffected. Consequently, the methane oxidation activity of $1\%Pt/ZrO_2$ will remain same and would continue parallel to the SO_2 oxidation process independently.

It is worth noting that the dipolar model presented in Fig. 9 to explain the high catalytic activity of Pt/ZrO_2 catalyst for methane oxidation can explain the high activity of Pt catalysts in methane oxidation reported previously [40–44]. In fact, these results suggest that the presence of surface platinum species in two different oxidation states is the key factor for high activity of platinum catalysts in methane oxidation.

It must be stated that while the formation of Pt ions at the surface of a semiconductor support is driven by the effect of energy alignment between the metal and the semiconductor, the oxidation state of Pt in the catalyst is also driven by the size of Pt particles, crystallographic orientation of the support, and preparation conditions of the catalyst. The subsequent interaction between the adsorbed CH_4 with adsorbed oxygen on the platinum nanoparticle surface, would result in the generation of CO_2 and H_2O molecules as final products.

The results presented in this investigation indicate that, the methane oxidation activity and the deactivation by sulfur poisoning of a Pt-supported semiconductor catalyst can be tuned by controlling the nature and relative concentrations of all possible dipolar catalytic sites at its surface.

4 Conclusions

Platinum-supported zirconia catalyst containing sub 2 nm Pt nanoparticles can be prepared by simple impregnation-calcination process. The high methane oxidation activity and stability of the $1\%Pt/ZrO_2$ catalyst is explained considering two important facts. The first fact, as suggested by XPS electronic state analysis of the catalyst, is the formation of highly stable Pt^{2+}–Pt^{4+} and Pt^{2+} –Zr^{4+} dipolar sites at platinum-support interface. The Pt^{2+}–Zr^{4+} sites present higher electric dipole potential than Pt^{2+}–Pt^{4+} sites. These dipolar sites strongly polarized CH_4 molecules, debilitating the C–H bond energy, and promoting the abstraction of the first hydrogen of adsorbed methane molecule, which is the rate determining step in the oxidation process. The second fact is that although, platinum surface is fully covered by oxygen molecules in the CH_4–O_2 reaction conditions (excess oxygen, 25–500 °C), preventing CH_4 adsorption, the rate of CH_4 adsorption at the dipolar sites is much higher than that of O_2 due to non-zero polarizability of methane and zero polarizability of O_2. Consequently, CH_4 oxidation proceed at relatively low temperature, despite of the presence of excess oxygen. The high stability of the catalyst during CH_4 oxidation in presence of SO_2 is associated to two factors: (i) due to higher electric dipole moment of SO_2 molecules than that of CH_4, they polarize more easily, and get adsorbed on dipolar

sites of the catalyst surface at higher rate; and (ii) most of the polarized SO_2 molecules are adsorbed on Pt^{2+}–Zr^{4+} dipolar sites, while the CH_4 molecules are adsorbed on Pt^{2+}–Pt^{4+} dipolar sites. Therefore, the SO_2 oxidation and CH_4 oxidation reactions at catalyst surface occur independently, without affecting each other. The high methane oxidation activity and high stability of the 1%Pt/ZrO_2 catalyst presented in this investigation show that the electronic state of platinum and its interactions with ZrO_2 are the key factors in methane oxidation process.

Acknowledgements The authors acknowledge Vicerrectoría de Investigación y Estudios de Posgrado (BUAP) (Grant No. Nat 2020-46), and Secretaría de Energía (Mexico) (Grant No. Cluster Biodiesel 250014), Consejo Nacional de CIencia y Tecnología (Mexico) (Grant No. Cluster Biodiesel 250014) for their financial supports.

References

1. Korakianitis T, Namasivayam AM, Crookes RJ (2011) Prog Energy Combust Sci 37:89
2. Allenby S, Chang WC, Megaritis A, Wyszyński ML (2001) Proc Instr Mech Eng D 215:405
3. Deutschmann O, Grunwaldt JD (2013) Chem Ing Tech 85:595
4. Farrauto RJ, Lampert JK, Hobson MC, Waterman EM (1995) Appl Catal B 6:263
5. Gélin P, Primet M (2002) Appl Catal B 39:1
6. Gärtner A, Lenk T, Kiemel R, Casu S, Breuer C, Stöwe K (2016) Top Catal 59:1071
7. Ciuparu D, Lyubovsky MR, Altman E, Pfefferle LD, Datye A (2002) Catal Rev 44:593
8. Gélin P, Urfels L, Primet M, Tena E (2003) Catal Today 83:45
9. M'Ramadj O, Zhang B, Li D, Wang X, Lu G (2007) J Nat Gas Chem 16:258
10. Osman AI, Abu-Dahrieh JK, Laffir F, Curtin T, Thompson JM, Rooney DW (2016) Appl Catal B 187:408
11. Corro G, Cano C, Fierro JG (2008) J Mol Catal A 281:179
12. Kylhammar L, Carlsson PA, Skoglundh M (2011) J Catal 284:50
13. Lampert JK, Kazi MS, Farrauto RJ (1997) Appl Catal B 14:211
14. Persson K, Ersson A, Manrique-Carrera A, Jayasuriya J, Fakhari R, Fransson T, Jaras S (2005) Catal Today 100:479
15. Sadokhina N, Smedler G, Nylén U, Olofsson M, Olsson L (2018) Appl Catal B 263:384
16. Gremminger A, Lott P, Merts M, Casapu M, Grunwaldt JD, Deutschmann O (2017) Appl Catal B 218:833
17. Platero EE, Mentruit MP, Areán CO, Zecchina A (1996) J Catal 162:268
18. Nakamoto K, Fujita J, Tanaka S, Kobayashi M (1957) J Am Chem Soc 79:4904
19. Larsen G, Lotero E, Nabity M, Petkovic LM, Shobe DS (1996) J Catal 164:246
20. Ciuparu D, Ensuque A, Shafeev G, Bozon-Verduraz F (2000) J Mater Sci Lett 19:931
21. Parida KM, Mallick S (2007) J Mol Catal A 275:77
22. Lietz G, Lieske H, Spindler H, Hanke W, Völter J (1983) J Catal 81:17
23. Lieske H, Lietz G, Spindler H, Völter J (1983) J Catal 81:8
24. Alerasool S, Boecker D, Rejai B, Gonzalez RD, Del Angel G, Azomosa M, Gomez R (1988) Langmuir 4:1083
25. Briggs D, Seah MP (1990) Practical surface analysis by auger and X-ray photoelectron spectroscopy, 2nd edn. Wiley, Chichester
26. Kim KS, Winograd N, Davis RE (1971) J Am Chem Soc 93:6296
27. Aricò AS, Shukla AK, Kim H, Park S, Min M, Antonucci V (2001) Appl Surf Sci 172:33
28. Barr TL, Yin MP (1989) ACS Symp Ser 411:203
29. Ardizzone S, Bianchi CL (1999) Appl Surf Sci 152:63
30. Miranda CD, Ramírez AE, Jurado SG, Vera CR (2015) J Mol Catal A 398:325
31. Deeba M, Farrauto RJ, Lui YK (1995) Appl Cat A 124:339
32. Bond GC (1962) Catalysis by metals. Academic Press, London
33. Godolets GI (1983) Stud Surf Sci Catal 15:365
34. Beck DD, Krueger MH, Monroe DR (1991) SAE Paper no. 910844
35. Ebitani K, Konishi J, Horie A, Hattori H, Tanabe K (1989) In: Tanabe K, Hattori H, Yamaguchi T, Tanaka T (eds) Acid-base catalysis. Kodansha, Tokyo, pp 491–498
36. Kikuchi R (2001) Environ Manag 27:837
37. Sulfur trioxide measurement technique for SCR units. Environment project No. 1885. October 2016. The Danish Environmental Protection Agency. Editor Fateev A and Calusen S. ISBN: 978-87-93529-18-2
38. Krakow B, Lord RC (1966) J Chem Phys 44:3640
39. Doornkamp C, Ponec V (2000) J Mol Catal A 162:19
40. Garetto TF, Apesteguía CR (2000) Cat Today 62:189
41. Fujimoto K, Ribeiro FH, Avalos-Borja M, Iglesia E (1998) J Catal 179:431
42. Burch R, Hayes M (1995) J Mol Catal A 100:13
43. Beck IE, Bukhtiyarov VI, Pakharukov IY, Zaikovsky VI, Kriventsov VV, Parmon VN (2009) J Catal 268:60
44. Ono LK, Yuan B, Heinrich H, Cuenya R (2010) J Phys Chem C 114:22119
45. Ahmadi M, Mistry H, Cuenya R (2016) J Phys Chem Lett 7:3519
46. Cargnello M, Doan-Nguyen VVT, Gordon TR, Diaz RE, Stach EA, Gorte RJ, Fornasiero P, Murray CB (2013) Science 341:771
47. Ozier I (1971) Phys Rev Lett 27:1329
48. Patel D, Margolese D, Dykea TR (1979) J Chem Phys 70:2740

Affiliations

Rosalía Torralba[1] · Grisel Corro[1] · Fer Rosales[1] · Fortino Bañuelos[1] · Umapada Pal[2] · Octavio Olivares-Xometl[3] · Emmanuel Guilleminot[4] · José Luis G. Fierro[5]

Umapada Pal
upal@ifuap.buap.mx

Octavio Olivares-Xometl
oxoctavio@yahoo.com.mx

Emmanuel Guilleminot
emmanuel.guilleminotco@udlap.mx

José Luis G. Fierro
jlgfierro@icp.csis.es

[1] Instituto de Ciencias, Benemérita Universidad Autónoma de Puebla, 4 sur 104, 72000 Puebla, Mexico

[2] Instituto de Física, Benemérita Universidad Autónoma de Puebla, Apdo. Postal J-48, 72570 Puebla, Mexico

[3] Facultad de Ingeniería Química, Benemérita Universidad Autónoma de Puebla, 4 sur 104, 72000 Puebla, Mexico

[4] Department of Physics, King's College, London WC2R 2LS, UK

[5] Instituto de Catálisis y Petroleoquímica, Cantoblanco, 28049 Madrid, Spain